A Testbed for experimental performance evaluation of Multicarrier Waveforms in presence of RF PA

R. Zayani*†, H. Shaïek†, C. Alexandre†, A. Kielys†, X. Cheng†, X. Fu† and D. Roviras†

* Innov'Com, Sup'Com, Carthage University, Tunis , Tunisia
†CEDRIC/LAETITIA, CNAM, Paris, France
{rafik.zayani, hmaied.shaiek, christophe.alexandre, daniel.roviras}@cnam.fr

***Abstract*—This paper presents an experimental testbed to evaluate the performance of CP-OFDM and the most promising 5G multicarrier waveforms (MWFs) WOLA-OFDM and BF-OFDM in presence of a real RF power amplifier (RF PA). In particular, we focus on the in-band and out-of-band non-linear distortions and their effects on power spectrum density (PSD) and bit error rate (BER), respectively. Testbed results are obtained in a realistic laboratory experimentation with configurable universal software radio peripherals (USRPs) based software defined radio (SDR) prototype. Testbed results confirm that different waveforms lose rapidly their good properties when non-linear RF PA is considered. Waveform performances are validated and compared via both simulations and experimental measurements.**

***Keywords*—5G, MTC, Multicarrier Waveforms, CP-OFDM, WOLA-OFDM, BF-OFDM, RF PA, Testbed.**

I. Introduction

The information and communication technologies (ICT) industry is making rapid progress toward fifth/next generation (5G) wireless networks [1], which aims to integrate almost everything across the globe into the internet, and achieve seamless and ubiquitous communications [2]. In this regard, the international telecommunication union radiocommunications (ITU-R) standardization Sector has categorized the usage scenarios for international mobile telecommunication (IMT) for 2020 and beyond into three main groups [3]: enhanced mobile broadband (eMBB), massive machine type communications (mMTC), and ultra-reliable and low latency communications (uRLLC). Specified target requirements to be fulfilled by IMT-2020-compliant radio access include 20 Gb/s peak data rate, 100 Mb/s user experienced data rate, $10Mb/s/m^2$ area traffic capacity, 10^6 devices$/km^2$ connection density, 1 ms latency and mobility up to 500 km/h [4]. To meet these design goals, the third generation partnership project (3GPP) has launched the standardization activity for the first phase 5G system in Release 15 named New Radio (NR) in 2016, targeting deployment in 2018 and the ready system in 2020 [5].

In this regard, work on 5G wireless communication technologies has been ongoing in academia and international projects for several years. Examples of the key technologies considered include massive multiple-input multiple-output (MIMO) (from legacy cellular frequency bands up to high frequencies), where the BSs are equipped with an excess of antennas to enhance both spectral-efficiency (SE) and energy-efficiency (EE) [1], enhanced multicarrier waveforms (MWF) flexibly accommodate various services/applications with different requirements [3], and so on.

It is unlikely that 5G challenges can be satisfied using Orthogonal Frequency Division Multiplexing (OFDM), the MWF adopted by physical layer (PHY) of todays long term evolution advanced (LTE-A). The post-OFDM MWF chosen must allow for specific 5G asynchronous signaling scenarios, support large bandwidth (100MHz and above), allow for high SE, support various multi-antenna techniques and flexible duplex, and allow for ultra-low latency, low-power and low-complexity design [3].

A first class of these MWFs gathers the ones that adopt a per-subcarrier pulse-shaping to reduce out-of-band (OOB) emission and increase bandwidth efficiency and relaxed synchronization requirements: generalized frequency division multiplexing (GFDM) [6] and filter-bank multi-carrier (FBMC) [6] have been heavily studied. The Universal filtered multicarrier (UFMC) [7] is another class of sub-band filtering based waveform, where only a transmit filter is used while the demodulation in the receiver relies on the oversampled discrete Fourier transform (DFT). Time-domain windowing can also be considered to achieve the desired enhancements, which is to prevent steep changes between two OFDM symbols so as to confine OOB emission. In this regard, an advanced windowing based waveform called - Weighted Overlap and Add based OFDM (WOLA-OFDM) [7] has been studied. This technique has lower complexity compared to that of filtering techniques [8]. It is worth mentioning that an agreement on the 5G waveform was reached by member companies of the 3GPP, which claimed that spectral confinement techniques such as filtering and windowing for a waveform at the transmitter should be transparent to the receiver [9] [10]. In this regard, an advanced block-filtered OFDM (BF-OFDM) has been introduced [11] in the sense that the receiver can be reduced to a simple FFT and therefore remains identical to the CP-OFDM one. Interested readers are referred to [12] for an overview as well as qualitative and quantitative comparisons among different waveforms. As 3GPP is one of the major contributors on the standards of global cellular networks for upcoming 5G, it is encouraged to concentrate on more careful and thoughtful design, evaluations, realizations and comparison of CP-OFDM waveform and its most promising enhancements, i.e. WOLA-OFDM and BF-OFDM especially in experimental testbed. It is worth to mention the following contributions:

- Zayani et al. [7] propose applications of WOLA-OFDM to enable asynchronous transmissions, which is shown to outperform UFMC.
- Gerzaguet et al. [8] compare the performances of WOLA-OFDM and BF-OFDM in terms of spectrum confinement, transmitter complexity and robustness in a typical multi-user asynchronous scenario.

978-1-5386-5005-9/18/$31.00

- In [13], authors describe field-test experiments carried out with an implementation of the BF-OFDM and the feasibility of the use of mixed numerologies for 5G.
- Guan et al. [14] report a field in time division duplex downlink (TDD-DL) conducted on a configurable testbed in a real-world environment for the performance evaluations of CP-OFDM, Windowing-OFDM and filtered-OFDM.

Despite the mentioned MWFs advantages, they still suffer from high Peak-to-Average Power Ratio (PAPR) of the modulated signal. Consequently, they lose rapidly their good frequency localisation properties when non-linear RF PAs are used. In this regard and compared to the above contributions, this paper presents an experimental testbed to evaluate the performances of the most promising candidate WFs WOLA-OFDM and BF-OFDM in presence of a real RF PA. In particular, we focus on the in-band and out-of-band non-linear distortions and their effects on PSD and BER, respectively. Testbed results are obtained in a realistic laboratory experimentation with configurable universal software radio peripherals (USRPs) based software defined radio (SDR) prototype.

The main contributions of this paper are: we focus our attention firstly on building a practical and flexibly configurable testbed, as a general platform for our research. Measurements using real-world equipments can be served to convince evidences of technologies feasibility. Through this testbed, we develop an approach to characterize a real RF power amplifier. We present further discussions and comparisons on the different waveforms CP-OFDM, WOLA-OFDM and BF-OFDM and we provide insights on the impact of in-band and out-of-band non-linear distortions caused by RF PA.

The rest part of this present paper is structured as follows. Section II provides an overview of the tesbed. In particular, the detailed baseband processing of CP-OFDM, WOLA-OFDM, BF-OFDM and the PA identification method are presented, respectively. In section III, testbed setup is introduced, parameter selections are defined and waveform performances are validated and compared via both simulations and experimental measurements. The relevant performance, in terms of PSD and BER, are discussed. Finally, the conclusion is given in section IV.

Notations : $\mathbb{E}[.]$ stands for the expectation operator and $(.)^*$ denotes the complex conjugate operation.

II. Testbed Overview

In this section, we provide an overview of the considered testbed architecture for experimenting the candidate technologies performance, with a special focus on baseband processing.

A. Overall Architecture

The testbed consists of a prototype base station (BS) and a prototype user equipment (UE) representing, respectively, Transmitter (Tx) and Receiver (Rx) side. These prototypes are built using SDR platforms, as depicted in Fig. 1 to demonstrate the functionality and evaluate the performance of the most promising multicarrier post-OFDM waveforms in presence of RF PA. For SDR hardware, a common design principle applies for both BS and UE implementations using Universal Software Radio Peripherals (USRPs), which integrate digital/IF/RF units. The USRPs have tunable carrier frequencies in the range of 400 MHz to 4.4 GHz and tunable transmission rates to 200 mega samples per second [15]. Each USRP is connected to a workstation with GNU-radio for configuration and uploading/downloading signal. The transmitter USRP (BS side) communicates with the receiver USRP (UE side) through a RF PA. This latter is a Pasternack PE15A4017 wideband medium PA with a bandwidth of 20 MHz to 3 GHz, P1dB of 29dBm and 27 dB Gain [16]. The baseband unit is responsible for digital algorithm realizations, e.g., QAM modulation, waveform generation and shaping, channel equalization, demodulation, etc. This unit is software-based and implemented using MATLAB. It is worth noticing that PAPR reduction and DPD modules are not considered and the channel is a wired one to clearly show the impact of RF PA on the performances of the studied multicarrier waveforms.

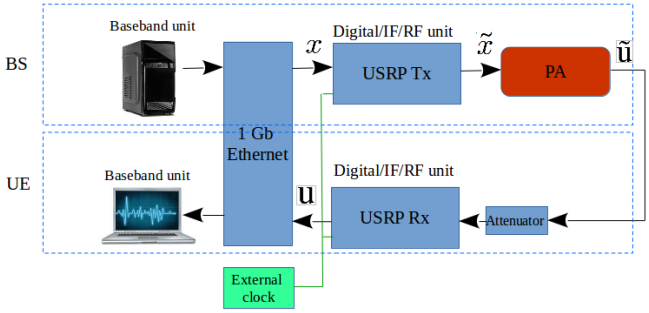

Fig. 1. Overall architecture.

B. Baseband Processing Procedure

In this section, the considered multicarrier WFs along with their associated transceivers are described.

1) Transceiver Structure: Figure 2 illustrates the software based basedband processing procedures on the BS (transmitter side) and the UE (receiver side). To emulate the coexistence of multiple numerologies, MCM Tx and MCM Rx stand for multicarrier modulation waveform at the transmitter side and receiver side, respectively. In the next subsections, we provide the baseband processing on these post-OFDM multicarrier waveforms : WOLA-OFDM and BF-OFDM, which are believed to be potential candidates for the physical layer of the future 5G MTC systems. The classical CP-OFDM will serve as a reference of comparison.

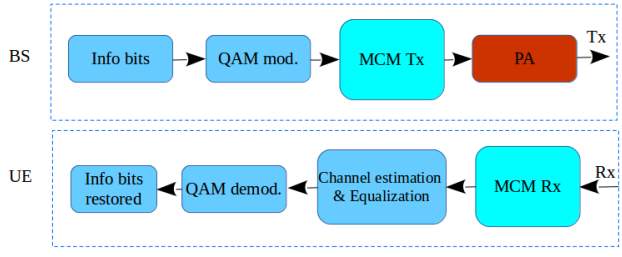

Fig. 2. Transceiver structure.

CP-OFDM: is adopted in several wireless standards (e.g. 3GPP-LTE and IEEE 802.11. a/g/n). Its key idea is to split up a stream of complex symbols at high-rate into several lower-rate streams transmitted on a set of orthogonal subcarriers which are

implemented using the inverse fast Fourier transform (IFFT). The OFDM transmitted signal can be written as,

$$\underbrace{\mathbf{x_n}}_{[N\times 1]} = \underbrace{\mathbf{F^{-1}}}_{[N\times N]} \underbrace{\mathbf{s_n}}_{[N\times 1]} \quad (1)$$

where, $\mathbf{F^{-1}}$ and $\mathbf{s_n}$ stand for the $N \times N$ IFFT matrix and a $N \times 1$ vector of complex input data symbols, respectively.

Accordingly, the OFDM receiver can be implemented using the fast Fourier transform (FFT). In order to prevent inter symbol interference (ISI), a cyclic prefix (CP) is usually inserted transforming thus the linear channel convolution into circular convolution if the CP is longer than channel impulse response. Therefore, after the FFT operation, the channel equalization becomes trivial through a single coefficient per subcarrier.

WOLA-OFDM: One notable difference of WOLA-OFDM is that, at the transmitter, the CP-OFDM modulated baseband signal is windowed by a well chosen window function. This aims to reduce the OOB emissions while maintaining the benefits of CP-OFDM. The WOLA-OFDM [17] has been intensively discussed for this purpose, and schemes have been proposed for asynchronous 5G [7] [8]. The performed time domain windowing aims to soften the edges at the beginning and the end of the rectangular filter response. These soft edges are added to the cyclic extensions of the OFDM symbol of length N. Indeed, the smooth transition between the last sample of a given symbol and the first sample of the next symbol is provided with point-to-point multiplication of the windowing function and the symbol with cyclic prefix and cyclic suffix. To create the cyclic prefix, we copy and append the N_{CP} samples from the last part of a given symbol to its beginning. Besides, the cyclic suffix consists in adding the first W_{TX} samples of a given symbol to its end. Thus, the WOLA-OFDM time domain symbol is cyclically extended from N samples to $L = N + N_{\mathrm{CP}} + W_{TX}$. After the cyclic extensions insertion, a window of length L is applied. The Meyer RRC [18] pulse combining the RRC time domain pulse with the Meyer auxiliary function has been demonstrated [7] to be a straightforward solution to define edge of the time domain window. Since, we have to comply within standards, adjacent symbols are overlapped in the edge transition region, which results in a similar overhead as in the classical CP-OFDM.

Although the transmit windowing is used to improve the spectral containment of the transmitted signal, an advanced windowing is also applied at the receiver side in order to enhance asynchronous inter-user interference suppression, as illustrated in [Fig.3 - 7]. The applied receive window is independent from the one applied at the transmitter and its length is equal to $N + 2W_{RX}$.

BF-OFDM: Block-Filtered OFDM (BF-OFDM) is a precoded filter-bank multi-carrier modulation that has been introduced in [19], [11]. The precoding stage is performed by means of CP-OFDM modulators and the filtering operation is applied with a polyphase network (PPN). The same precoding scheme was first proposed for FFT-FBMC, introduced in [20], that results in complex receiver scheme. The key idea of BF-OFDM is to slightly increase the transmitter complexity in order to rely on a low-complex CP-OFDM like receiver through the insertion of a filter pre-distortion stage at the transmitter side [13]. Indeed, the transmitter is composed of M CP-OFDM modulators feeding a filter bank. In order to ensure proper recovering, only $P/2$ subcarriers per OFDM modulator bear the data. The allocation of the active subcarriers depends on the parity of the carrier index and is performed by the framing stage. Then, the extra additional pre-distortion stage aims at compensating the distortion induced by the filter (in both amplitude and phase) inside the carrier bandwidth in order to flatten the received signal spectrum at the receiver side. The receiver is simply composed of a $MP/2$-point FFT. No filtering stage is required at the receiver side thanks to the pre-distortion stage added at the transmitter side. Hence, the receiver scheme is very similar to the one used in legacy CP-OFDM. It is worth mentioning that the rejection of interferences caused by filter bank are controlled by both the filter shape and the CP. This provides a signal-to-interferences ratio (SIR) of about 60dB that does not disturb the transmission over the other carriers [12].

2) PA nonlinearity: An important element in the transmit chain of the SDR is the RF power amplifier which amplify the transmitted signal to power levels detectable by the receivers. For high energy efficiency, the PA should be operated close to its saturation region (non-linear region of operation). However, this could drive the device to produce severe amplitude (AM/AM) and phase (AM/PM) distortions. This is the key impairment in multicarrier techniques based communication systems, since these latter suffer from the high PAPR. Introduced nonlinearity leads to spectral re-growth (out of band distortions) outside the allocated bandwidth thus violating the spectral mask. Further, in-band distortions introduced by the nonlinear behaviour of the PA causes increased bit error rate (BER). The AM/AM and AM/PM characteristics indicate the relationship between, respectively, the modulus and the phase variation of the output signal as functions of the modulus of the input one. Then, the amplified signal $u(n)$ can be written as [21]

$$u(n) = F_a(\rho)\exp(jF_p(\rho))\exp(j\phi) \quad (2)$$

where $F_a(.)$ and $F_p(.)$ stand, respectively, for the AM/AM and AM/PM characteristic and ρ and ϕ are the modulus and phase of the input signal.

A popular choice for modeling these nonlinear PA characteristics is the Volterra series [22]. However, due to the high model complexity, truncated versions are used in practice, where the polynomial model provides good tradeoff between complexity and performance. For a bandpass nonlinear system only the odd order nonlinearities affect the signal component close to the carrier [23] [24], i.e. the frequency region that the equivalent lowpass models describe. Using the standard polynomial formulation and imposing the quasi-static constraint results in the lowpass model that referred to as an odd-even model [24]

$$u(n) = \sum_{p=1}^{R} c_p x(n)|x(n)|^{(p-1)} \quad (3)$$

where $x(n)$ is the input signal, R is the number of coefficients and c_p are the complex-valued polynomial coefficients. Usually, c_p are found in the time domain, either on a sample-by-sample basis using algorithms like least mean squares (LMS) [25] or least squares (LS) [26]. In this paper, we consider this polynomial model to identify our PA, which has been demonstrated to provide good performance [25] and allow further analytical performance analysis [21]. Modeling will be performed using data measured on the considered RF PA through our experimental platform.

TABLE I. TESTBED PARAMETERS

General	
Data frequency band	$2.0020 - 2.0030$ GHz
Sampling rate (F_s)	10 MHz
Frame length	0.1 ms
Symbols/Frame	1000
Data Constellation	16-QAM
CP-OFDM / WOLA-OFDM	
FFT size	2048
CP length	72
Windowing	Meyer Raised cosine
Window length (W_e,W_r)	$(20, 20)$
BF-OFDM	
M	64
P	64
N_{CP}	4
K	4
Prototype filter	Gaussian, BT=$1/3$

III. EXPERIMENTAL RESULTS AND VALIDATION

A. Experimental Setup

Measurements using the testbed introduced in previous section were performed in order to evaluate the performance of studied multicarrier waveforms in presence of nonlinear RF PA. They are built around a system setup that, first, identifies a behavioral model of the PA in subsequent steps, and then validates it by comparing simulated results and the measured ones. A brief summary of testbed setups and parameters is provided in Table I.

The test signal used was an OFDM one of 10 MHz bandwidth and PAPR of 11 dB, modulated at 2 GHz. It was decided that data occupies about 1 MHz bandwidth from 2.0020 to 2.0030 GHz. This arrangement allows us a clean an observation bandwidth of three times the main data bandwidth, which is sufficient to see all spectral components generated by the amplifier under test. The validation and identification signals were different but of same bandwidth and PAPR. It is worth mentioning that only CP-OFDM waveform was considered for identification while all studied waveforms were served for validation.

B. Modeling a Measured PA

A digital representation of the PA output envelope is made available to the baseband processing unit using the observation path. The PA output is attenuated, down-converted to IF and converted to baseband using USRP Rx module (see Fig. 1). Then, the data is filtered using a bandpass filter to reject the unwanted hardware (HW) imperfections like DC component and IQ imbalance. The bandwidth of this filter should at least be three times the transmit data bandwidth that will allow us to observe spectral components generated by nonlinearities up to degree three. The polynomial model in equation (3) was considered using 2048×10^3 samples for both transmit and receive baseband signals and it was evaluated for $R = 20$.

An important condition for proper estimation is that the sequences $x(n)$ and $u(n)$ are time-aligned. Various elements (analog and digital) in the experimental testbed introduce arbitrary loop delay for the observed signal. Correlation based techniques can be used to estimate and compensate the delay to the accuracy of one frame that will serve to the PA modeling. It is worth mentioning that due to the external synchronisation used for the USRP Tx and USRP Rx modules, the CFO does not exist. Real power amplifier and the estimation algorithm are assumed to operate on scaled version of $\tilde{x}(n)$ and $\tilde{u}(n)$ of the PA input and output, respectively. Indeed, the observation path introduces scaling to the observed PA input and output. These effects can be modelled as scaling by real constants g_{TX} and g_{RX}, respectively. g_{TX} is estimated as follows

$$g_{TX} = \sqrt{\frac{\frac{10^{PindBm/10}}{10}}{\mathbb{E}\left[|x(n)|^2\right]}} \tag{4}$$

where $PindBm$ denotes the average power at the input of the real PA, which is measured using a spectrum analyzer.

g_{RX} is estimated from the time aligned samples $u(n)$ and the scaled $\tilde{x}(n)$, using a linear observation path, as

$$g_{RX} = \sqrt{\frac{\mathbb{E}\left[|u(n)|^2\right]}{\mathbb{E}\left[|\tilde{x}(n)|^2\right]}} \tag{5}$$

These estimates are used to compute, respectively, $\tilde{x}(n) = g_{TX}x(n)$ and $\tilde{u}(n) = g_{RX}u(n)$, which then are used by the estimation algorithm as well as the polynomial PA model. The AM/AM and AM/PM conversion curves of this PA are shown in Fig. 3. We recall that these curves are found from measurements using the Pasternack PE15A4017 wideband medium PA [16]. The 1dB compression point (P1dB) is also marked on this plot. In order to validate our approach, the performance of the three considered WFs, in terms of PSD and BER, using this estimated polynomial model (i.e. simulated using MATLAB) are compared to the measured ones performed using our experimental testbed in conjunction with the real PA.

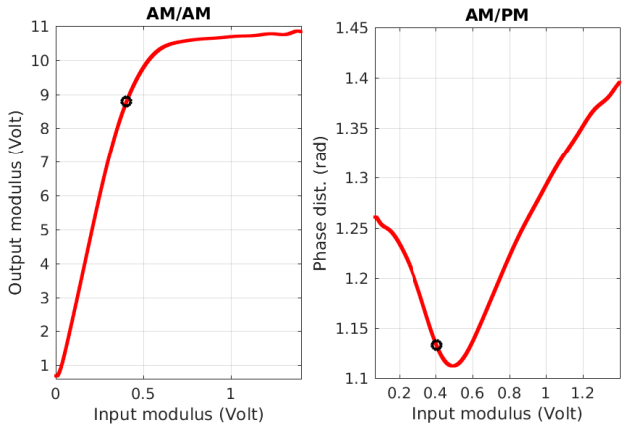

Fig. 3. AM/AM and AM/PM conversions for PA used. The black circle marked on the plots correspond to the 1dB compression point (P1dB)

C. PSD

Figs 4.a, 4.b and 4.c show the simulated and measured (observed on Agilent ESA E4405B) spectra of the PA outputs for the three MWFs CP-OFDM, WOLA-OFDM and BF-OFDM, respectively. $IBO = xDB - sim$ and $IBO = xDB - mes$ are, respectively, used to indicate simulated and measured results in presence of PA for a given input back-off (IBO) value. $IdealPA - sim$ denotes results in a linear case. We consider an observation bandwidth of three times the main data bandwidth, centred at one channel bandwidth away from the data bandwidth on either side. According to these results, we can clearly see a very good agreement between simulated spectra and measured ones in the case of all the considered WFs. This can confirm that our PA identification method was efficient and the identified model reflects exactly the actual functioning of the real RF

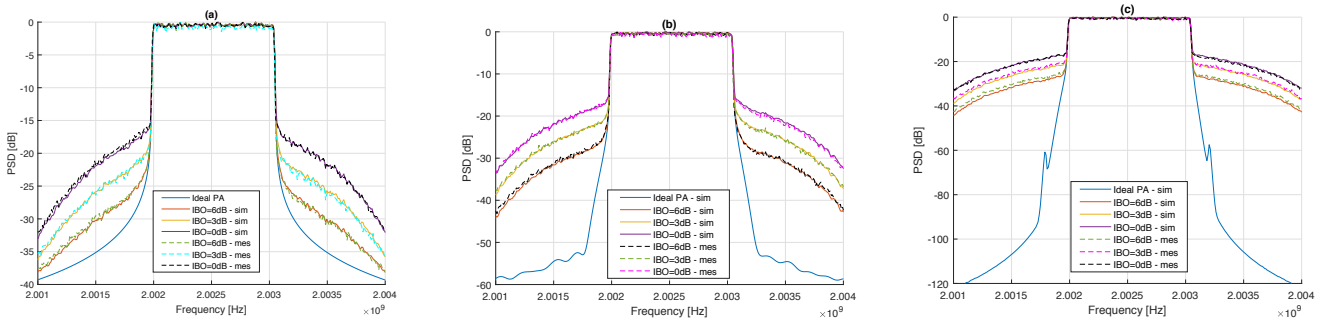

Fig. 4. PA output spectra for (a) CP-OFDM (b) WOLA-OFDM (c) BF-OFDM

PA. We take advantage to evaluate the out-of-band distortions caused by the RF PA on the considered multicarrier waveforms, we show in Figs 5.a and 5.b the spectra comparison of the three WFs for, respectively, an IBO of 3dB and 6dB. We note that all waveforms have been strongly affected when a RF PA is used with an IBO=3dB, even the advanced ones (WOLA-OFDM and BF-OFDM). They lose rapidly their good properties of reduced OOB emissions and perform as the CP-OFDM. For IBO=6dB, a gain is performed by these advanced waveforms compared to CP-OFDM. Further, we note a negligible gain for BF-OFDM compared to WOLA-OFDM, which is due to the better spectrum containment provided by the subband filtering used by BF-OFDM.

D. BER

In-band error is measured in terms of the bit error rate (BER) computed at the receiver side (performed by MATLAB). In order to clearly see the effect of our RF PA and without loss of generality, noise is added at this level and its power level (N_0) is adjusted to have the desired E_b/N_0. Again, we can see from Fig 6.a that simulated and measured curves are in good agreement in the case of all waveforms. Only the CP-OFDM case is considered to make the presentation clear but same behaviors have been made in cases of WOLA-OFDM and BF-OFDM. These results confirm again the validity of our identified PA model.

We can note further, from results depicted in Fig 6.b, that WOLA-OFDM and BF-OFDM provide the same performance compared to the classical CP-OFDM. This can demonstrate that RF PA nonlinearities cause a serious problem for the post-OFDM WFs. Thus, these imperfections have to be taken into account in the system design and advanced solutions have to be studied in order to has the properties of good frequency localization of post-OFDM WFs.

IV. Conclusion

Research, development and standardization activities for the 5G are in full action. As a fundamental component, the underlying post-OFDM waveform is expected to be able to support the coexistence of diverse services. In this paper, we provide details and guidance on the experimental tesbed design and implementation to evaluate the performances of the most promising post-OFDM waveforms. In particular, we conduct a testbed to compare different 5G waveform candidates, i.e. WOLA-OFDM and BF-OFDM in the presence of RF power amplifier. Testbed results show that the AM/AM and AM/PM non-linear distortions affect strongly the performance, in terms of frequency localization, of the studied WFs. It is shown that these multicarrier WFs almost perform as the classical CP-OFDM when PA is operated near its saturation region (e.g. where the energy efficiency is high). Based on the testbed results, a higher attention must be paid for RF PA effects that should be taken into account in the design of the next 5G WFs.

References

[1] K. N. R. S. V. Prasad, E. Hossain, and V. K. Bhargava. Energy efficiency in massive mimo-based 5g networks: Opportunities and challenges. *IEEE Wireless Communications*, 24(3):86–94, June 2017.

[2] C. X. Wang, F. Haider, X. Gao, X. H. You, Y. Yang, D. Yuan, H. M. Aggoune, H. Haas, S. Fletcher, and E. Hepsaydir. Cellular architecture and key technologies for 5g wireless communication networks. *IEEE Communications Magazine*, 52(2):122–130, February 2014.

[3] Y. Liu, X. Chen, Z. Zhong, B. Ai, D. Miao, Z. Zhao, J. Sun, Y. Teng, and H. Guan. Waveform design for 5g networks: Analysis and comparison. *IEEE Access*, 5:19282–19292, 2017.

[4] S. Y. Lien, S. L. Shieh, Y. Huang, B. Su, Y. L. Hsu, and H. Y. Wei. 5g new radio: Waveform, frame structure, multiple access, and initial access. *IEEE Communications Magazine*, 55(6):64–71, 2017.

[5] M. Shafi, A. F. Molisch, P. J. Smith, T. Haustein, P. Zhu, P. De Silva, F. Tufvesson, A. Benjebbour, and G. Wunder. 5g: A tutorial overview of standards, trials, challenges, deployment, and practice. *IEEE Journal on Selected Areas in Communications*, 35(6):1201–1221, June 2017.

[6] C. Kim, Y. H. Yun, K. Kim, and J. Y. Seol. Introduction to qam-fbmc: From waveform optimization to system design. *IEEE Communications Magazine*, 54(11):66–73, November 2016.

[7] Rafik Zayani, Yahia Medjahdi, Hmaied Shaiek, and Daniel Roviras. WOLA-OFDM: a potential candidate for asynchronous 5g. In *IEEE Global Communications Conference (GLOBECOM)*, 2016.

[8] R. Gerzaguet, Y. Medjahdi, D. Demmer, R. Zayani, J. B. Dor, H. Shaiek, and D. Roviras. Comparison of promising candidate waveforms for 5g: Wola-ofdm versus bf-ofdm. In *2017 International Symposium on Wireless Communication Systems (ISWCS)*, pages 355–359, Aug 2017.

[9] RAN1 Chairmain's Notes, document 3gpp tsg ran wg1 meeting 86, gothenburg, sweden,.

[10] RAN2 Chairmain's Notes, document 3gpp tsg ran wg1 meeting 86bis, lisbon, portugal,.

[11] Robin Gerzaguet, David Demmer, Jean-Baptiste Doré, and Dimitri Kténas. Block-Filtered OFDM: a new promising waveform for multi-service scenarios. In *submitted to IEEE ICC 2017 (ICC)*, Paris, France, May 2017.

[12] Y. Medjahdi, S. Traverso, R. Gerzaguet, H. Shaek, R. Zayani, D. Demmer, R. Zakaria, J. B. Dor, M. Ben Mabrouk, D. Le Ruyet, Y. Lout, and D. Roviras. On the road to 5g: Comparative study of physical layer in mtc context. *IEEE Access*, 5:26556–26581, 2017.

[13] R. Gerzaguet, S. Bicais, P. Rosson, J. Estavoyer, X. Popon, D. Dassonville, J. B. Dore, B. Miscopein, M. Pezzin, D. Miras, and D. Ktenas. 5g multi-service field trials with bf-ofdm. In *2017 IEEE Globecom Workshops (GC Wkshps)*, pages 1–5, Dec 2017.

[14] P. Guan, D. Wu, T. Tian, J. Zhou, X. Zhang, L. Gu, A. Benjebbour, M. Iwabuchi, and Y. Kishiyama. 5g field trials: Ofdm-based waveforms and mixed numerologies. *IEEE Journal on Selected Areas in Communications*, 35(6):1234–1243, June 2017.

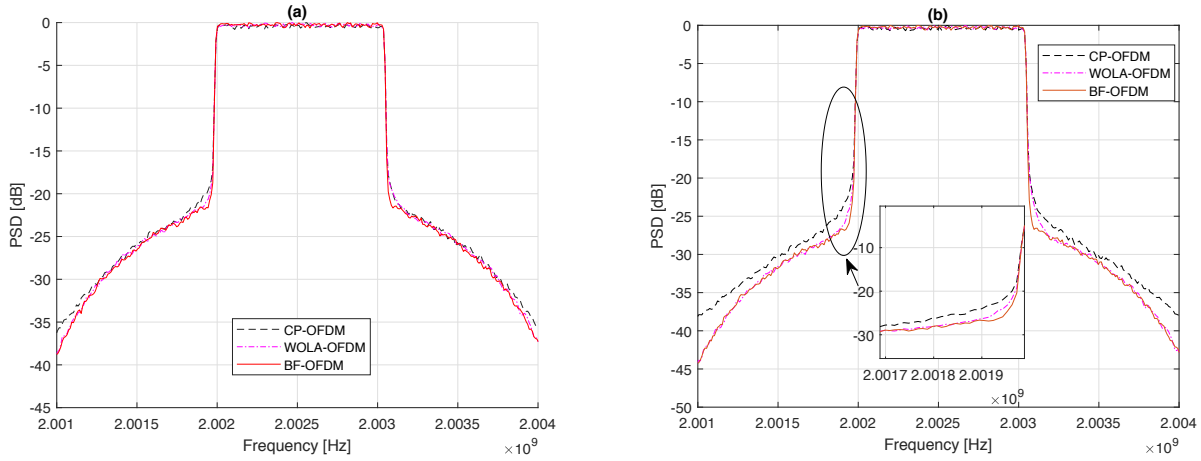

Fig. 5. PA output spectra for different WFs with (a) IBO=3dB (b) IBO=6dB

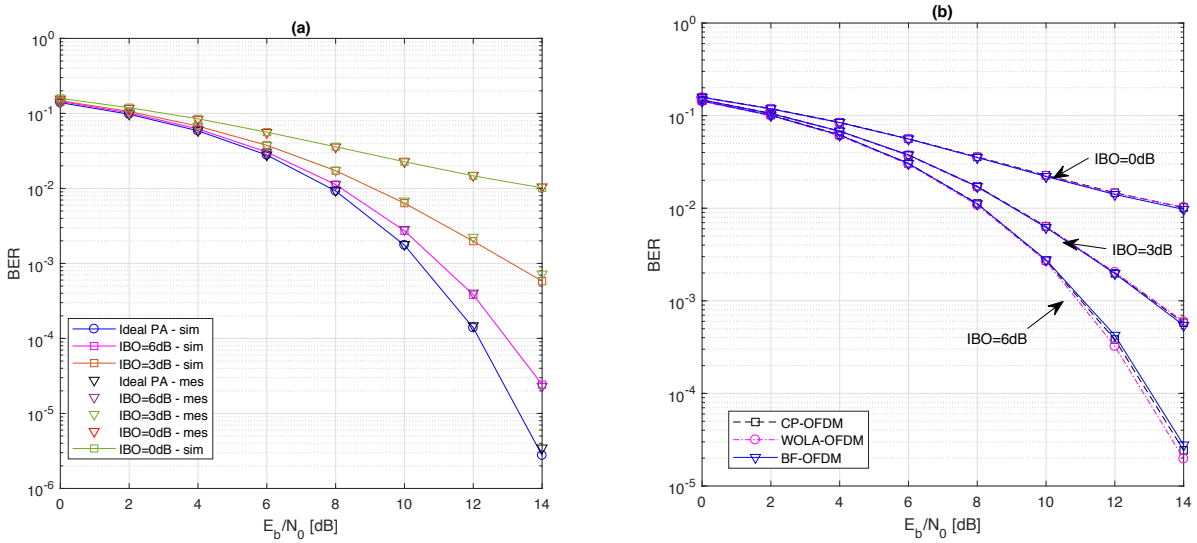

Fig. 6. BER vs E_b/N_0, 16-QAM, IBO=$\{0, 3, 6\}$ (a) CP-OFDM (b) different WFs

[15] USRP-2942 Specifications, available at: https://www.ni.com/pdf/manuals/374410d.pdf.

[16] Pasternack PE15A4017, available at: https://www.pasternack.com/images/productpdf/pe15a4017.pdf.

[17] Qualcomm, Incorporated. R1-162199 - Waveform candidates.

[18] I. Gaspar, M. Matth, N. Michailow, L. Leonel Mendes, D. Zhang, and G. Fettweis. Frequency-shift offset-qam for gfdm. *IEEE Communications Letters*, 19(8):1454–1457, Aug 2015.

[19] David Demmer, Robin Gerzaguet, Jean-Baptiste Doré, Didier Le Ruyet, and Dimitri Kténas. Block-Filtered OFDM: an exhaustive waveform to overcome the stakes of future wireless technologies. In *submitted to IEEE ICC (ICC)*, Paris, France, May 2017.

[20] R. Zakaria and D. Le Ruyet. Theoretical Analysis of the Power Spectral Density for FFT-FBMC Signals. *IEEE Communications Letters*, 20(9):1748–1751, Sept 2016.

[21] Hanen Bouhadda, Hmaied Shaiek, Daniel Roviras, Rafik Zayani, Yahia Medjahdi, and Ridha Bouallegue. Theoretical analysis of ber performance of nonlinearly amplified fbmc/oqam and ofdm signals. *EURASIP Journal on Advances in Signal Processing*, 2014(1):60, 2014.

[22] Schetzen M. The volterra and wiener theories of nonlinear systems. 2006.

[23] K. K. S. Pillai, S. Sagar, S. K. Parambeth, and N. Prem Krishnan. Implementation of digital pre-distortion for power amplifier linearisation in software defined radio. In *2017 Twenty-third National Conference on Communications (NCC)*, pages 1–6, March 2017.

[24] P. N. Landin and D. Rnnow. Rf pa modeling considering odd-even and odd order polynomials. In *2015 IEEE Symposium on Communications and Vehicular Technology in the Benelux (SCVT)*, pages 1–6, Nov 2015.

[25] D. Zhou and V. E. DeBrunner. Novel adaptive nonlinear predistorters based on the direct learning algorithm. *IEEE Transactions on Signal Processing*, 55(1):120–133, Jan 2007.

[26] Lei Ding, G. T. Zhou, D. R. Morgan, Zhengxiang Ma, J. S. Kenney, Jaehyeong Kim, and C. R. Giardina. A robust digital baseband predistorter constructed using memory polynomials. *IEEE Transactions on Communications*, 52(1):159–165, Jan 2004.

V. Acknoledgment

This work has been performed in the framework of the WONG5 project, receiving funds from the French National Research Agency (ANR) under the contract number ANR-15-CE25-0005-02.